ParCFD2024
35th International Conference on Parallel Computational Fluid Dynamics
Sep. 02-04, 2024, Bonn, Germany

Wet-Surface Modeling in Lattice-Boltzmann Simulations for Evaluating Surgery Impacts on the Humidity Transfer in Nasal Flows

Shota Ito[a,*], Mario Rüttgers[b], Moritz Waldmann[c] and Andreas Lintermann[b]

[a]Karlsruhe Institute of Technology, Lattice Boltzmann Research Group, Institute for Mechanical Process Engineering and Mechanics, Englerstraße 2, 46131, Karlsruhe, Germany
[b]Forschungszentrum Jülich GmbH, Jülich Supercomputing Centre, 52458, Jülich, Germany
[b]RWTH Aachen University, Chair of Fluid Mechanics and Institute of Aerodynamics, Aachen, Germany

ARTICLE INFO[†]

Keywords:
Lattice Boltzmann Method;
Nasal Cavity Flows;
Humidity Transport;
Turbinectomy

ABSTRACT

A numerical study using the lattice-Boltzmann method is conducted to investigate the conditioning ability of the human nose, where a boundary treatment is implemented to model the latent heat effect. The humidity exchange at the wet surface of the nasal mucosa influences the wall temperature, imitating the thermal inertial effects of the mucosa tissue. To capture the curvature of the cavity geometry, interpolated bounce-back schemes are used to set the wall temperature and water concentration computed by the boundary model. The impact of evaporation on the conditioning ability is investigated for pre- and post-surgery cavity geometries of a patient that was diagnosed with enlarged turbinates and underwent turbinectomy. The widening of the nasal passages in the course of the turbinectomy cause a reduced pressure loss between the inlets (nostrils) and the outlet (pharynx), but also dry air streaming towards the back part of the airway-throat interface. This coincides with the patient's perception, who reported less efforts for breathing in, but at the same time a dry and sometimes painful feeling at the back of the throat.

1. Introduction

Clinical investigations of the conditioning ability of the nose demonstrate a challenge due to the difficult access of the nasal cavity with measurement equipment. Computational fluid dynamics (CFD) enables in-depth studies of the nasal conditioning ability, allowing to obtain velocity, pressure, temperature, and humidity concentration distributions inside the cavity. The lattice Boltzmann method (LBM) has proven to be a popular approach to address fluid flow problems in the medical field [1, 2] due to the adaptability towards complex geometries and easy extension to solve transport phenomena.

This article presents numerical studies on the influence of the latent heat effect of evaporation on the inhalation process through the nose. The nasal cavity geometry is obtained via computer tomography scans converted into a surface model with the automated machine learning-based pipeline described in [3]. CFD simulations are conducted for the pre- and post-surgical anatomy of a patient that underwent turbinectomy, a surgical intervention to treat enlarged turbinates. Whereas previous attempts for estimating and planning surgical interventions with an LBM mainly focus on a surgery's influence on the pressure or temperature distributions [4, 5], the current study allows to analyze the main complication of a turbinectomy, i.e., a decreased capability to humidify incoming air. On the one hand, turbinectomy is known to reduce nasal resistance and ease breathing [6]. On the other hand, it alters nasal conditioning, since less heat exchange and humidification are possible, resulting in streams of significantly colder and dryer air in the nasopharynx [7].

2. Numerical Method

For solving each macroscopic equation, i.e., Navier-Stokes equation (NSE) for the airflow and advection-diffusion equations (ADE) for the heat and humidity transfer, the LBM implemented in the open source multiphysics solver framework m-AIA [1] (multiphysics - Aerodynamisches Institut Aachen, formerly known as Zonal Flow Solver (ZFS) [8]) is employed where the temperature and water concentration distribution are computed via passive scalar transport. The velocity discretization model is the D3Q27 lattice and the second-order equilibrium distribution is used for the BGK-collision operator for all solved equations. The boundary treatment for the NSE system, in- and outflow for the ADE systems are chosen similarly as in [5]. The interpolated

[†]This paper is part of the ParCFD 2024 Proceedings. A recording of the presentation is available on YouTube. The DOI of this document is 10.34734/FZJ-2025-02479 and of the Proceedings 10.34734/FZJ-2025-02175.

*Corresponding author
shota.ito@kit.edu (S. Ito); (M. Rüttgers); (M. Waldmann); a.lintermann@fz-juelich.de (A. Lintermann)
ORCID(s): 0000-0002-6946-0203 (S. Ito); 0000-0003-3917-8407 (M. Rüttgers); 0000-0001-7895-761X (M. Waldmann); 0000-0003-3321-6599 (A. Lintermann)

[1] https://git.rwth-aachen.de/aia/MAIA/Solver

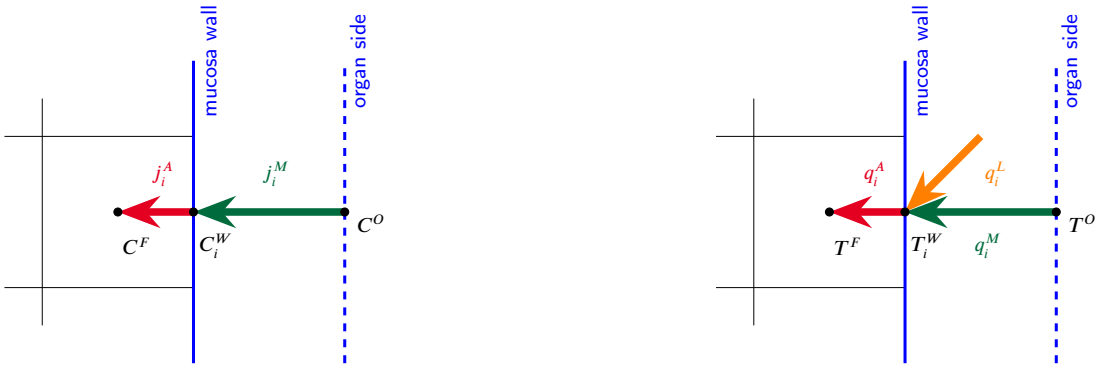

(a) Water flux at the mucosa wall

(b) Heat flux at the mucosa wall

Figure 1: The heat and water flux are evaluated at the mucosa wall to obtain the temperature and concentration at the wall. The computed latent heat flux depends on the passed water flux from the mucosa to the fluid.

bounce-back scheme for the ADE [9] is applied for the heat and humidity transport to compute the missing boundary populations to account for the boundary curvature of the nasal cavity wall, i.e.,

$$g_{\bar{i}}(\mathbf{x}, t+\Delta t) = \begin{cases} -2q\tilde{g}_i(\mathbf{x},t) + (2q-1)\tilde{g}_i(\mathbf{x}-\mathbf{c}_i\Delta t, t) + \frac{1}{4}\Phi_i^W & , \mathrm{q} < 0.5 \\ -\frac{1}{2q}\tilde{g}_i(\mathbf{x},t) + \frac{2q-1}{2q}\tilde{g}_{\bar{i}}(\mathbf{x},t) + \frac{1}{8q}\Phi_i^W & , 0.5 \le q \le 1 \end{cases}, \quad (1)$$

where q is the normalized distance between the boundary node and wall intersection point in the discrete velocity direction i, and Φ_i^W the desired value for the wall temperature T^W and water concentration C^W prescribed by the scheme. This scheme uses neighboring populations and the exact boundary distance in contrast to the simple bounce-back scheme which enables to prescribe Φ_i^W at the boundary wall.

In order to compute Φ_i^W, the wet surface model from [10] is used. The wet surface model assumes an additional outer layer with a uniform thickness in the normal direction to the geometry wall, modeling the nasal mucosa, which is referred to as the membrane layer. The temperature at the outside wall of the membrane layer is called the organ-side temperature T^O, which is assumed to be constant due to the continuous heat supply by the blood capillaries. For the same reason, the organ-side water concentration C^O is assumed to be fully saturated at the outer layer. To approximate C^O, the fully saturated water concentration of air as a function of the temperature T is computed via $C = w\rho T$, where ρ is the density of air and w is the water fraction (kg water vapor per kg dry air), given by the empirical function [10, 11]

$$w(T) = \frac{1}{1000} \cdot (2.027 + 0.0006312T^3 - 0.010972T^2 + 0.6036T). \quad (2)$$

To compute the missing wall temperature T^{W} and water concentration C^{W}, the energy and mass balance at the nasal wall are evaluated as depicted in Fig. 1. The heat flux q and water flux j are computed by using linear approximations for the gradients, i.e., the fluxes on the membrane side are

$$q_i^M = k^M \frac{T^O - T_i^W}{\delta_i^M} \quad \text{and} \quad (3)$$

$$j_i^M = D^M \frac{C^O - C_i^W}{\delta_i^M}, \quad (4)$$

where k^M is the heat conductivity, D^M is the diffusivity constant of water, and δ_i^M is the distance in the membrane layer along the discrete velocity direction. At the opposite side of the nasal cavity wall, the airflow, heat, and concentration transport are simulated. The heat and water flux from a boundary lattice node with the fluid cell temperature T^F and water concentration C^F to the wall are approximated by

$$q_i^A = k^A \frac{T_i^W - T^F}{\delta_i^A} \quad \text{and} \quad (5)$$

$$j_i^A = D^A \frac{C_i^W - C^F}{\delta_i^A}, \quad (6)$$

where δ_i^A is the distance between the fluid cell center and the wall surface in the opposite discrete velocity direction of the missing population. Note, that in Eq. (6) the convective part is neglected due to the assumption of low flow velocities in the wall vicinity. An additional term in the energy balance is introduced, which imitates the heating and cooling of the mucous layer due to condensation and evaporation, respectively. The heat flux of the latent heat is computed by $q_i^L = -j_i^A h_i^L$, where h_i^L is the specific latent heat in kJ/kg, given as a function of the temperature [11]

$$h^L(T) = 2500.8 - 6.1434 \cdot 10^{-6} \cdot T^3$$

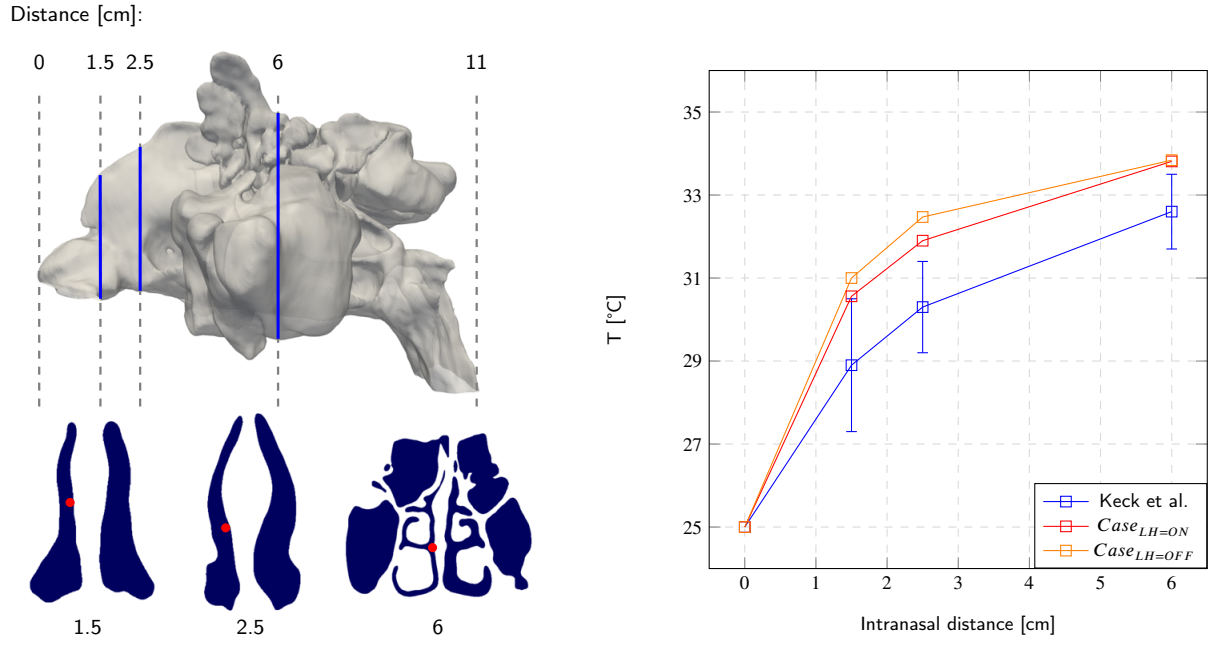

(a) Intranasal positions.

(b) Mucosa surface temperature.

Figure 2: Comparison of the intranasal mucosa temperature concentration at the positions 1.5 cm, 2.5 cm, and 6 cm between the simulation and measurements from [12]. The influence of the latent heat effect is shown.

$$+ 1.5893 \cdot 10^{-3} \cdot T^2 - 2.3641 \cdot T. \qquad (7)$$

Evaluating the energy and mass balances as $q_i^A = q_i^M + q_i^L$ and $j_i^A = j_i^M$ along the missing population direction yields the missing wall values Φ_i^W for Eq. (1).

3. Results

The wet surface model was first sanity-checked in a wet pipe flow simulation in [13], similarly as in [10, 11]. Then, the impact of the latent heat on the mucosa surface is compared against the experimental data of [12]. That is, the nasal mucosa temperature is compared at three nasal locations shown in Fig. 2. Therein, it is shown that by considering the latent heat effect, the simulated nasal mucosa temperature approaches the trend of the experimental results. Note that a perfect match is not to be expected, since the nasal cavity model in the current study is different from the model in [12]. More details regarding the conducted tests of the wet surface model are given in the work of [13].

The flow simulations were conducted on 8 nodes of the graphics processing unit (GPU) partition of JURECA-DC [14], i.e., on a total number of 32 NVIDIA A100 GPUs. Traditionally, m-AIA was developed to run CFD simulations in parallel on central processing unit (CPU) partitions of high-performance computing (HPC) systems. However, recently GPU partitions on HPC systems are gaining popularity. To allow computations on both partitions, the lattice-Boltzmann method has been ported to GPUs using the *parallel Standard Library* (pSTL) algorithms of C++17 in combination with NVIDIA's NVHPC compiler.

The simulation domain is resolved by about $220 \cdot 10^6$ cells, using mesh resolutions of $\Delta x = 0.1\ mm$. The grid resolution is finer than the spatial resolution of the CT data to resolve all relevant flow features to analyze the flow. Especially thin wall-bounded shear layers which are relevant to simulate the right heat transfer are resolved accurately this way [1]. The patient has undergone turbinectomy in the left nasal passage (from the patient's view).

The surgical intervention reduces the total pressure loss between the inlets (nostrils) and outlet (pharynx) from 10.02 Pa before the surgery to 7.11 Pa afterwards (−31%). At the same time, the temperature difference between the incoming air at the inlets and outlet is reduced from 304.8 K to 295.8 K (−3%), and the humidity concentration from 96.2% to 90.0% (−7%). Figure 3a illustrates the total pressure loss to the inflow areas for a cross-sectional area through the left nasal passage. It is clearly shown how the removal of parts of the inferior and middle turbinates widen the nasal passage and, therefore, decrease the pressure loss. Figure 3b shows the humidity distribution for the same

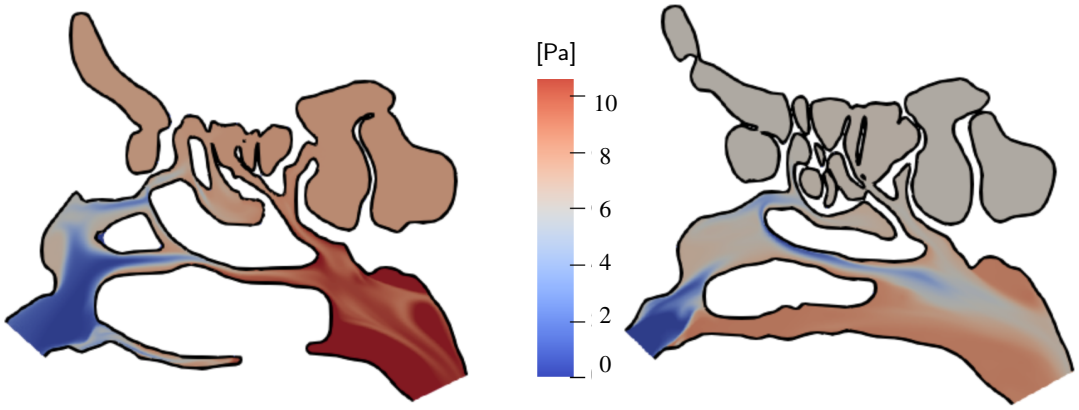

(a) Total pressure loss to the inflow areas (nostrils) for a cross-sectional area through the left nasal passage (from the patient's view) of the pre-surgical (left) and the post-surgical (right) cases.

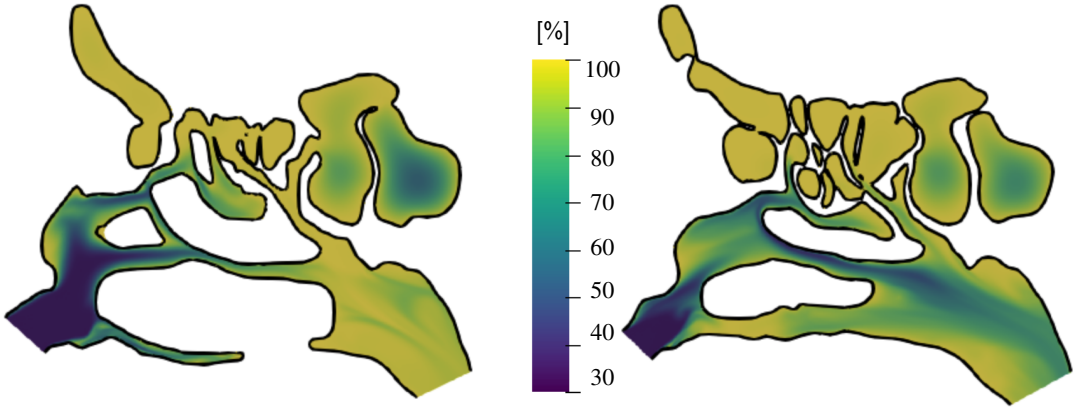

(b) Humidity distribution for a cross-sectional area through the left nasal passage (from the patient's view) of the pre-surgical (left) and the post-surgical (right) cases.

cross-sectional area. The narrowed passages in the pre-surgical case allow closer contact between the incoming air and the airway-nose interface, and, therefore, an increased heat exchange and humidification. In contrast, the widening of the nasal passages in the course of the turbinectomy cause dry air streaming towards the back part of the airway-throat interface. This coincides with the patient's perception, who reported less efforts for breathing in, but at the same time a dry and sometimes painful feeling at the back of the throat.

4. Acknowledgements

The research leading to these results has been conducted in the HANAMI project, which receives funding from the European Union Horizon Europe Programme - Grant Agreement Number 101136269 under the call HORIZON-EUROHPC-JU-2022-INCO-04. The authors gratefully acknowledge the computing time granted by the JARA Vergabegremium and provided on the JARA Partition part of the supercomputer JURECA [14] at *Forschungszentrum Jülich*. The authors would like to thank the patient for providing the computer tomography data.

References

[1] A. Lintermann, M. Meinke, W. Schröder, Fluid mechanics based classification of the respiratory efficiency of several nasal cavities, Computers in Biology and Medicine 43 (11) (2013) 1833–1852. doi:10.1016/j.compbiomed.2013.09.003.

[2] M. Waldmann, A. Lintermann, Y. J. Choi, W. Schröder, Analysis of the Effects of MARME Treatment on Respiratory

Flow Using the Lattice-Boltzmann Method, 2020, pp. 853–863. doi:10.1007/978-3-030-25253-3_80.

[3] M. Rüttgers, M. Waldmann, W. Schröder, A. Lintermann, A machine-learning-based method for automatizing lattice-boltzmann simulations of respiratory flows, Applied Intelligence 52 (2022) 9080–9100. doi:10.1007/s10489-021-02808-2.

[4] M. Waldmann, M. Rüttgers, A. Lintermann, W. Schröder, Virtual surgeries of nasal cavities using a coupled lattice-boltzmann–level-set approach, Journal of Engineering and Science in Medical Diagnostics and Therapy 5 (3) (2022). doi:10.1115/1.4054042.

[5] M. Rüttgers, M. Waldmann, K. Vogt, J. Ilgner, W. Schröder, A. Lintermann, Automated surgery planning for an obstructed nose by combining computational fluid dynamics with reinforcement learning, Computers in Biology and Medicine 173 (2024) 108383. doi:10.1016/j.compbiomed.2024.108383.

[6] X. Chen, S. Leong, H. Lee, V. Chong, D. Wang, Aerodynamic effects of inferior turbinate surgery on nasal airflow - a computational fluid dynamics model, Rhinology 48 (2010) 394–400. doi:10.4193/Rhino09.196.

[7] J. Siu, K. Inthavong, J. Dong, Y. Shang, R. G. Douglas, Nasal air conditioning following total inferior turbinectomy compared to inferior turbinoplasty – a computational fluid dynamics study, Clinical Biomechanics 81 (2021) 105237. doi:10.1016/j.clinbiomech.2020.105237.

[8] A. Lintermann, M. Meinke, W. Schröder, Zonal flow solver (ZFS): a highly efficient multi-physics simulation framework, International Journal of Computational Fluid Dynamics 34 (7-8) (2020) 458–485. doi:10.1080/10618562.2020.1742328.

[9] L. Li, R. Mei, J. F. Klausner, Boundary conditions for thermal lattice boltzmann equation method, Journal of Computational Physics 237 (2013) 366–395. doi:10.1016/j.jcp.2012.11.027.

[10] S. Hanida, F. Mori, K. Kumahta, M. Watanabe, S. Ishikawa, T. Matsuzawa, Influence of latent heat in the nasal cavity, Journal of Biomechanical Science and Engineering 8 (3) (2013) 209–224. doi:10.1299/jbse.8.209.

[11] K. Inthavong, D. F. Fletcher, M. Khamooshi, S. Vahaji, H. Salati, Wet surface wall model for latent heat exchange during evaporation, International journal for numerical methods in biomedical engineering 38 (4) (2022) e3581. doi:10.1002/cnm.3581.

[12] T. Keck, R. Leiacker, H. Riechelmann, G. Rettinger, Temperature profile in the nasal cavity, The Laryngoscope 110 (4) (2000) 651–654. doi:10.1097/00005537-200004000-00021.

[13] S. Ito, Implementation of a humidity transport equation for the analysis of the nasal airfow using a lattice-boltzmann method, Master's thesis, Institute of Aerodynamics and Chair of Fluid Mechanics, RWTH Aachen University (2022).

[14] D. Krause, P. Thörnig, JURECA: Modular supercomputer at Jülich Supercomputing Centre, Journal of Large-scale Research Facilities 4 (2018) A132. doi:10.17815/jlsrf-4-121-1.